

Characterization of Semi-crystalline Polymers Using MRI

Apostolos Kantzas^{1,2} and David Axelson³

1: Department of Chemical and Petroleum Engineering, University of Calgary, Alberta, Canada T2N 1N4, akantzas@ucalgary.ca.

2: Tomographic Imaging and Porous Media Laboratory, Calgary, Alberta Canada T2N 1N4.

3: MR_Consulting, Kingston, Ontario, Canada K7L 4V1, axelsond@chem.queensu.ca.

Abstract – ¹H single point magnetic resonance imaging (SPI)[1],[2],[3] has been introduced in the literature as a method for determining relaxation characteristics of semi-crystalline polymers and for extracting MRI images from such samples. The work presented in the literature to date demonstrates the applicability of this technique. In this work, SPI has been applied to the direct observation of stress-induced changes, temperature induced changes and structural changes in the apparent spin-spin relaxation time, T_2^* , in polyethylene samples. Several samples prepared under quite different conditions were studied.

Keywords: MRI, polymers, SPI, stress/strain, T_2^*

1. INTRODUCTION

The characterization of stresses in materials is a critical component in the process of understanding material behavior and failure under service conditions. The development of rapid and accurate diagnostic techniques for screening stress distributions in fabricated polymeric products would undoubtedly enhance manufacturers' ability to optimize various processes and to better comprehend the origins and mechanisms of product failures. For instance, an understanding of failure processes in the 'brittle' mode below yield stress is very important for the prediction of pipe service lifetime[4],[5]. The problem is to predict when material will fail under a given set of loading conditions. While yielding is determined by stresses acting throughout a section of a component and can be calculated, fracture is controlled by cracks and other defects which may be visually undetectable; brittle fracture occurs before the material is able to yield. Environmental stress cracking phenomena have also been described extensively in the literature [6]. The mechanisms of failure involve the nucleation of small voids, the formation of crazes, and the subsequent growth and fracture of these crazes [7]. The resistance to slow crack growth of polyethylene materials, as measured by the time to failure, can vary by more than a factor of 10^6 , depending on the morphological and molecular structure [4],[7].

When a polymer is stressed the relative degree of molecular mobility decreases, there is

an increase in relative orientation, reduced molecular mobility, and (possibly) stress induced crystallization. How these phenomena correlate with the measurement of various NMR-derived parameters in various polymers of interest has only recently become the (successful) subject of study.

NMR has the potential to be of significance in quality control and process development studies. For instance, internal stresses are a primary cause of shrinkage and warpage in injection-molded parts and are suspected to be responsible for environmental stress cracking[8]. Internal stress can also result from rapid inhomogeneous cooling of a polymer melt; during initial cooling surface layers will stiffen sooner than the core region and subsequent solidification and thermal contraction of the core produces residual stresses[9]. Stresses in surface regions are considered to be very difficult to determine, but as shown here, are amenable to study by magnetic resonance imaging with the proper protocols.

Correlations between MRI/NMR - derived transverse relaxation (T_2 , T_2^* , T_2^{eff}) parameters and stress-strain have clearly shown that fundamental correlations exist for rubbery materials[10][11]. However, imaging of stressed semi-crystalline polymers poses particularly difficult experimental problems for NMR imaging. Extensive broad-line NMR analysis of a series of predominantly high density polyethylene products[12] showed that the amorphous, interfacial and crystalline components have average T_2^* 's of about 111 μs , 31 μs and 5 μs ,

respectively, at ambient temperature. These data establish the basic time scale (under ambient conditions) for the characterization of spin-spin relaxation in these materials. Not only are the T_2^* 's inherently short to begin with, they can be expected to become significantly shorter as stress increases. The significance and strength of these relationships is being investigated to address such concerns as: what relaxation time regimes must be characterized for various materials, do methods exist to adequately (quantitatively) characterize these relaxation times, and what limitations exist on sample sizes with respect to the available methods.

Semi-crystalline polymers crystallized from the melt usually consist of lamellar crystalline regions separated by non-crystalline regions. At least three distinct regions can be assumed for semi-crystalline polymers, the relative proportions of which may vary greatly in samples of different structure and thermal history. In particular, we can define a crystalline region, an interfacial (transition) region, and an amorphous (or inter-zonal) phase. The crystalline component comprises chain sequences in ordered or preferred conformations. The interfacial region is diffuse and ill defined, being many monomer units thick with crowded and/or distorted segmental packing. A variety of structures within the interfacial phase may be envisioned, including loose chain segments attaching one part of a crystallite to the same crystallite, tight loops, chain ends terminating in the interfacial or amorphous zones, and tie molecules (both taut and loose) connecting different crystallites. In the fully disordered, amorphous state the polymer chains assume their characteristic random (liquid-like) configurations. The properties of the polymer reflect the relative number, type, and distribution of these chain entities. The rigidity of a semi-crystalline, thermoplastic polymer is mainly a function of its crystalline content. The density of a high density polyethylene correlates with its mechanical properties such as yield strength and small deformation properties like torsional stiffness, and Young's modulus, irrespective of the average molecular weight of the polymer, but dependent on the co-monomer content. The amorphous region, together with the crystalline region control the mechanical properties.

Of relevance to our study is the assumption that any relaxation in response to local stresses in the structure should mainly occur by rearrangement of molecular segments and movement of molecules in the amorphous phase, with accompanying elastic relaxation of stress in the crystalline regions. This implies that characterization of the transverse relaxation time of the crystalline components is not of primary

concern to an understanding of the stress and fracture processes. This does not imply that this component is irrelevant to our understanding of material responses to stress, only that the major changes in structure, orientation and mobility are expected to occur in the non-crystalline phases. Furthermore, given that the inherent relaxation times of the crystalline phase are short (i.e., $< 10 \mu\text{s}$) any changes in physical and morphological state that result in shorter relaxation times will lead to little or no significant changes in the crystalline phase values since these entities are already close to or at their limits of molecular immobilization with respect to the types of measurements we are making here and their associated error limits. For this reason and the experimental fact that it is very difficult to reliably quantify the crystalline component via SPI imaging methods we have chosen to generally consider the longer time transverse relaxation behavior in these samples, i.e., $T_2^* > 15 \mu\text{s}$.

Our prime interest is to use MRI to map out the spatial distribution in 2D or 3D of relevant NMR relaxation times that are related to the physical and/or mechanical properties of semi-crystalline polymers. The SPI method [1],[2],[3] gives access to the most rigid phases present and the concomitant use of variable temperature MRI gives additional flexibility in controlling T_2 values in complex systems.

For most elastomers T_2 of ^1H is predominantly determined by motional averaging of the homonuclear dipole-dipole interactions. Such molecular motions are, for instance, reorientation and slow translation of chain segments which have correlation times shorter than 10^{-8}s and slow chain dynamics with τ_c of the order of 10^{-8}s . Thus T_2 is a suitable parameter for analysis of molecular dynamics and therefore are expected to be dependent on cross-link density and applied strain. Changes in molecular mobility and thus changes in T_2 can be introduced by application of external forces in straining the sample. This effects a change in free volume and orientational alignment in the elastomer network by the packing of inter-cross-link segments [12].

The ability to measure relaxation properties of polymer objects under stress was demonstrated in a series of tests presented below. Moreover, relaxation data for a number of polyethylene and polypropylene samples at different temperatures were collected and analyzed using a bi-exponential and a tri-exponential model. The bi-exponential model assumes that the sample consists of two phases (one crystalline and one non-crystalline), while the tri-exponential model assumes that the sample consists of three phases (one crystalline, one transition and one non-crystalline). Each model predicts some

characteristic T_2 relaxation time for each phase in the polymer. Although studies involving variable temperature MRI have appeared, none involve MRI of semi-crystalline polymers. This is a consequence of the lack of available accessories from any commercial vendor and the difficulty of imaging such rigid solids without specialized techniques.

2. EXPERIMENTAL

All experiments were performed using Single Point Imaging (SPI) [1],[2],[3]. Unless otherwise noted, typical experimental conditions for the experiments were as follows: A 70 mm ^1H probe in the BG15 gradient set was used for samples with diameters less than about 6 cm. All data were acquired with the Bruker Biospec 24/30 system, operating at 100 MHz.

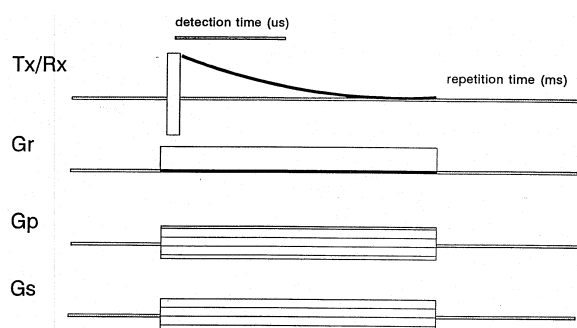


Figure 1: Single Point Imaging. Gr refers to read, Gp refers to phase and Gs refers to slice gradients

The schematic of the single point (constant time) imaging algorithm is given in Figure 1. The associated parameters are: field of view $3 \times 3 \text{ cm}^2$, acquisition matrix $32 \times 32 \rightarrow 128 \times 128$, reconstruction matrix size 128×128 , sweep width 100-500 kHz, pulse length $5 \mu\text{s}$, number of averages 2-8, detection time $17 \mu\text{s} - 2000 \mu\text{s}$, repetition time 40 ms, gradient strengths 5-80 % of maximum values, total experimental time 4 min/image with up to 18 images per data set and gradient power supply duty cycle $< 1\%$.

Through SPI images of T_2^* relaxation times are created. The analysis of the decay data on a pixel by pixel basis is fit using single- bi- and tri-exponential models. As a result, and depending on the model, a variety of T_2^* maps are created (short, intermediate, long). The changes in these maps, with structure, temperature and stress are addressed.

This protocol is different in many respects from all other NMRI techniques used. The acquisition matrix size can be a non-power of two value (which is subsequently zero filled to any other desired power of two). This allows the user extremely fine control over such critical parameters as gradient strength, resolution, duty

cycle and experimental time. This is more important for SPI than most other methods due to the (sometimes) very high gradient strengths explicitly required to image rigid solids.

Relaxation time calculations were performed using the following methodology. The raw series of images obtained as a function of detection time were acquired, concatenated into a single file and normalized. These 32 bit transformed image data were then imported into a personal computer-based, image processing package written in house. Each pixel was analyzed assuming various models for the decay rates. For the high signal-to-noise ratio pixels in the centre of the image a two or three component exponential decay was obtained while those pixels characterized by low(er) signal-to-noise ratios at the edges of the image were characterized by single exponential decays and/or Gaussian modified exponential decays with one or two time constants.

Variable temperature data acquisitions were performed with in-house designed and constructed equipment with the following features: sufficiently non magnetic to be used within 1 meter of the 2.35 Tesla, 30 cm bore horizontal magnet without any detectable change in resonance frequency, easy access for modification and sample insertion/displacement, no decreased image signal due to pumps/fans/etc., vacuum jacketed and water-cooled glass enclosure into which the probe is inserted to ensure probe stays at the stable ambient temperature, several fail-safe devices to ensure that water supply and temperature regulation desired are actually maintained, extremely well insulated so that sample temperature is always equal to the set point temperature with known air flows and proper equilibration times (estimated temperature variation $\pm 2^\circ\text{C}$). Maximum achievable temperatures are about 150°C .

The ability to characterize subtle differences is also a function of slice thickness, field of view, matrix size, gradient strength, echo time, etc., all of which can be further optimized to suit the situation at hand and the needs of the user. Relative low resolution 2D and 3D images (32^2 or 32^3 matrix sizes) also contain a considerable amount of useful information from the point of view of defect characterization and quality control analysis as these data may be acquired relatively rapidly.

Complementary bench-top NMR broad-line measurements were made with a Bruker NMS120 operating at a proton frequency of 20 MHz. Experimental conditions were as follows: number of scans; 10, bandwidth; broad, digitizer

resolution; high, gain; 68, detection mode magnitude; fid, detection 256 data points.

The advantages of variable temperature MRI have been demonstrated in the literature. Jerrard et al. [16] studied samples of a highly cross-linked polymer with T_g less than the ambient temperature, a rigid polyvinyl-acetate and a nylon-66 sample that have been diffused with water. T_2 values increased to varying degrees over the temperature range of ambient to 380°K. Changes were smallest for the elastomer (1.1 ms to 1.7 ms) and largest for the nylon (1.5 ms to 10 ms). Kauffman and Dybowski [17] reported the decomposition of the proton NMR spectra of linear, high molecular weight polyethylene over the temperature range of 133°K to 373°K. The Lorentzian component behaviour was studied in detail to yield transition temperatures associated with the γ - and α - transitions.

The variable temperature tests were performed using a variety of polyethylene and polypropylene samples. A brief description of each sample is given in Table 1.

The variable stress tests include MRI of standard tensile bars that were elongated up to 700%, a carbon black filled commercial gas pipe that was pressurized to failure and was analyzed as a function of radial distance from the burst point and several pellets, resins and components of automotive parts.

Code	Description	Size(μ m)	Density(g/cm^3)
G1#60	Impact PP I	375	0.8951
G1#10	Impact PP I	3000	0.8870
PP006	PP	pellet	0.8710
PE-1	PE	pellet	0.9369
PE-2	LLPDE	pellet	0.9169
J2#60	LLPDE II	375	0.9189
G2#60	Impact PP II	375	0.9001
J2#18	LLPDE II	1500	0.9210
M2#120	HDPE II	187.5	0.9481
M1#10	HDPE I	3000	0.9442
M1#P	HDPE I	37.5	0.9454
G1#35	Impact PP I	750	0.8916
G2#35	Impact PP II	750	0.8971

Table 1: Polyolefin Samples Used in MRI Experiments

3. RESULTS AND DISCUSSION

3.1. Variable temperature tests

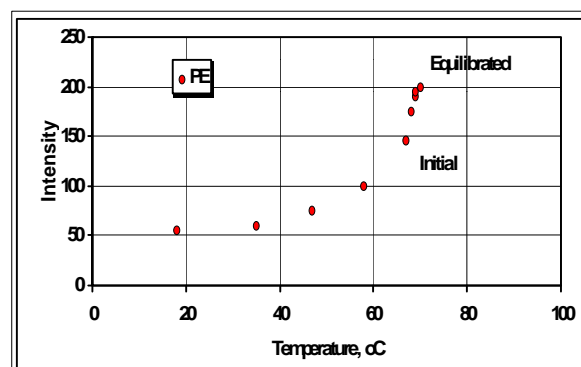


Figure 2: Typical plot of intensity magnification through heating for polyethylene

Figure 2 shows the relative difference in Intensity for a PE sample heated from 18°C to about 70°C for a fixed detection time of 120 μ s. There is approximately a 400% increase in signal-to-noise in this range. The effect of equilibration time on signal-to-noise is also shown in this figure at 70°C. The series of data points corresponds to measurements taken at about 5 min intervals until no further increase in intensity was observed. This illustrates that proper experimental protocols must be employed to ensure that all measurements are made under equilibrium conditions. The temperature dependence of the average T_2 values for samples G1#10 and G1#60 is shown in Figure 3 for the crystalline component (CC) over the range of 18°C to 150°C, while the corresponding plot for the non-crystalline component (NCC) is given in Figure 4. For the two samples G1#10 and G1#60 the T_2 for the NCC increases monotonically with increasing temperature. There are only small or negligible differences in T_2 for the NCC over the majority of the temperature range were investigated, with a small difference becoming evident only for the highest temperature used. T_2 values at 17°C/18°C were essentially identical before and after heating to 150°C, indicating no significant annealing effects (consistent with the literature to date). Differences in T_2 CC are more complex. First the range of T_2 values observed differs significantly between the two samples. More importantly, the change in T_2 with increasing temperature is not monotonic as some samples exhibit a very broad maximum in the range of 80-110°C. This can be possibly attributed to changes to molecular motion changes.

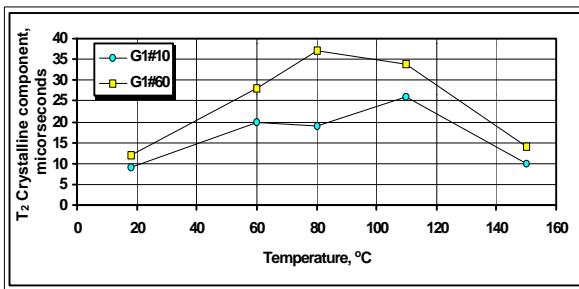


Figure 3: Effect of temperature on the T₂ crystalline component of polypropylene sample G1

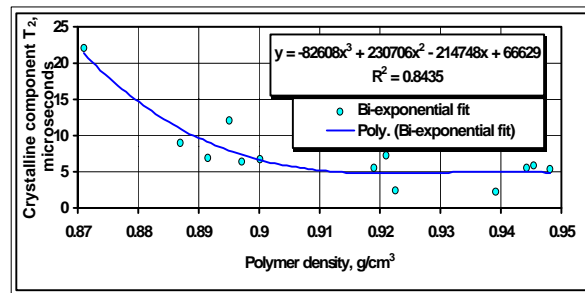


Figure 5: Effect of polymer density on the T₂ crystalline component of relaxation times

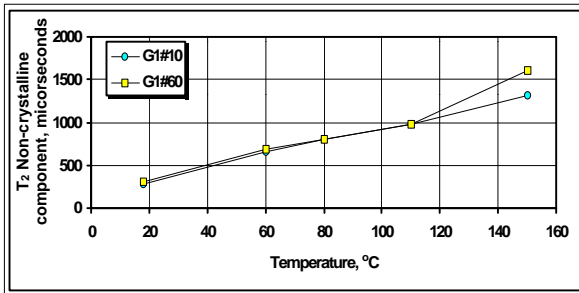


Figure 4: Effect of temperature on the T₂ non-crystalline component of polypropylene sample G1

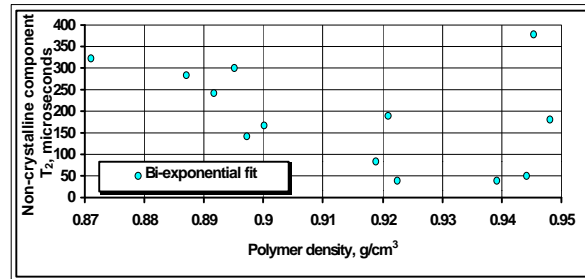


Figure 6: Effect of polymer density on the T₂ non-crystalline component of relaxation times

The tremendous advantage of measuring relaxation times in an imaging experiment is that we can now superimpose the calculated relaxation times on the pixels from which they were derived. NMS120 measurements and the like are always averages over large volumes of sample and subtle differences in relaxation time values as a function of location in the sample are lost. Under ideal conditions it would be possible to map out both relaxation time data (related to mechanical properties) and morphological data including the distributions of phases (mass fractions) in 2-D and 3-D. In a 3-D analysis of these samples it is possible to achieve resolutions in all three dimensions on the order of 100 μm in experimental times of 3-4 hours.

Figures 5 and 6 show the plots of relaxation time components with resin density. In Figure 5 the trends for the non-crystalline (long) component are shown. In Figure 6 the crystalline (short) component shows a decreasing trend up to density of 0.94, after which the relaxation times increase with increasing density. The quantification of such terms needs further investigation.

3.2. Tensile bar tests

Four of the elongated tensile bar samples are discussed here. Sample descriptions are as shown in Table 2.

Sample #	Total Length (cm)	Disturbed Length (cm)
1	13.1	2.0
2	15.3	4.8
3	19.0	9.5
4	23.8	15.0

Table 2: Properties of tensile bars

Upon stretching a sample, a substantial part of the plastic deformation occurs in an unstable way. This plastic instability manifests itself in the form of a neck which localizes at some region of the material and then spreads along the length of the specimen. Two regions develop: an unnecked region and a necked one with a transition zone dividing these two regions, commonly termed the shoulder, or the transition front. The sample then subsequently resists further extension and the neck stabilizes at this point. It then extends by drawing fresh material from tapering regions on either side until the whole parallel section of specimen has yielded. Two opposing forces can affect this process: dissipation of mechanical energy as heat and/or deformation resistance of the neck which has a higher strain rate than the surrounding polymer. Finally the sample fails. However crack propagation is invariably accompanied by certain amount of localized yielding over restricted area near crack tip, termed craze formation. For this preliminary evaluation, samples were not kept in

their fully stressed state, but were allowed to relax after initially being stressed.

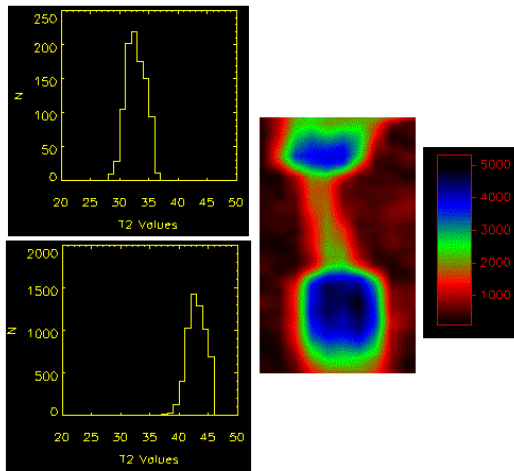


Figure 7: SPI images of a polyethylene tensile bar

On the left hand side of Figure 7 two histograms are shown, the top associated with the most strained region of the sample and the bottom with the least strained region(s) of the tensile bar. T_2^* 's are shifted to lower values with increasing strain. The image to the right side is that of the equilibrium intensity, M_0 , image associated with the display of the spin density independent of the relaxation time. However, as we have deliberately acquired data with detection times longer than about $3 \times T_2^*$ (crystalline component) we are actually mapping the equilibrium intensities of the non-crystalline components with $T_2^* > 5 \mu s$. The bar at the far right side displays the corresponding color codes associated with quantification of the image. The spin density decreases dramatically during drawing.

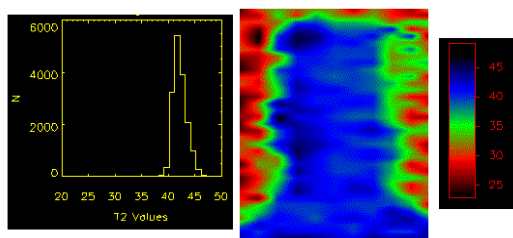


Figure 8: MRI of sample #2 in the least strained region

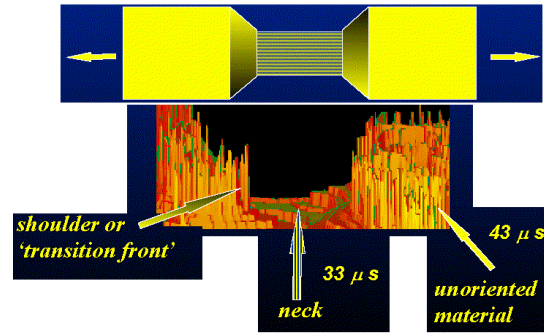


Figure 9: Schematic of MRI results for full sample #3

In another sample strained to greater degrees (Figure 8) we display the unnecked, least strained region again showing both the T_2^* histogram and the corresponding T_2^* map and color coding. The distribution of T_2^* 's sampled here is relatively narrow.

Figure 9 shows a schematic representation of the T_2^* relaxation time distribution in the necked, transition and unstressed end regions of sample III. The transition region is sharp.

3.3. Gas pipe tests

A carbon black filled polyethylene pipe (medium density, length=200mm, outer diameter =35mm, wall thickness=2.98mm) was sealed at both ends at then filled with water under increasing pressure until failure (at about 3.4MPa). The wall thickness at the burst point was reduced to 0.495mm.

The relaxation time decay rate was observed to be a function of the radial distance from the burst point in the pipe. The further away from the burst point the longer the T_2^* . Because of signal to noise limitations and as-yet undetermined effects of orientation on the relaxation time values, the numbers shown here are averages over the areas indicated in Figures 10-12, so these differences represent gross changes in the relaxation time behavior of each region.

To obviate the need for direct observation of rigid solids, investigators have used the presence of a mobile extrusion aid as the basis for imaging polyethylene pipes and noted that plasticizers and waxes might also be imaged with relatively little difficulty. The direct approach however, eliminates the need for suitable additives and avoids the problem of possibly insufficient signal to noise due to lack of additives.

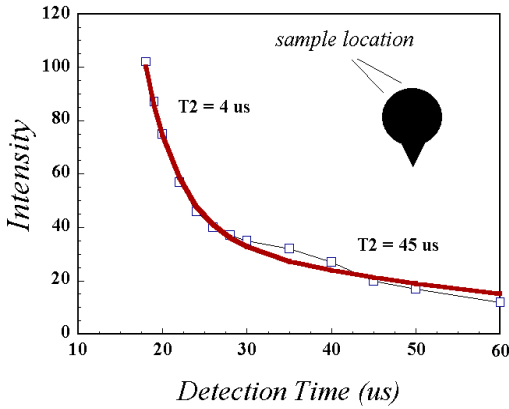


Figure 10: Relaxation decay for pipe sample furthest removed from burst point

Figure 10 shows the relaxation decay for the pipe sample furthest removed from the burst point. A bi-exponential decay fits the data best, but due to the insufficiently short detection time we do not place too much significance on the exact value for this short relaxation component. Figure 11 shows the relaxation time decay for the material at the burst point. A single exponential decay best fits the data. Finally, Figure 12 is a plot of relaxation time, T_2^* , versus radial distance from burst point.

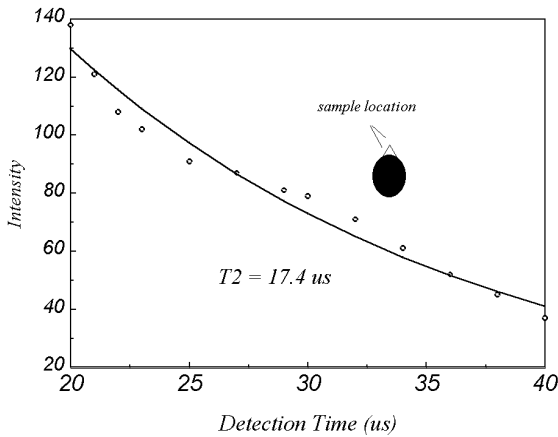


Figure 11: Relaxation time decay for the material at burst point

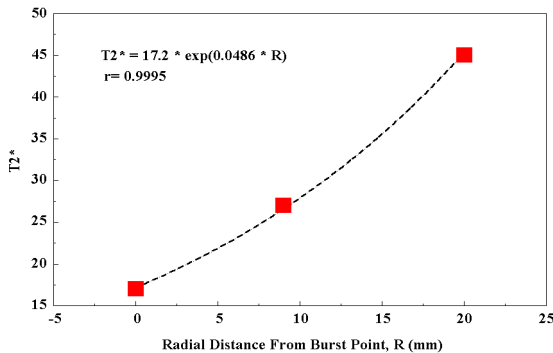


Figure 12: Plot of relaxation time T_2^* versus radial distance from burst point

The presented preliminary results can be used to shed light on the creation of deformations in semi-crystalline polymers under stress. There is need for further work in this area to quantify the mechanisms of such processes. Such an attempt is currently under investigation in our laboratory. MRI can be used to study deformation of polymer materials and perhaps help identify the magnitude of the residual stresses on a polymer product., (i.e., possibly create a data base for such systems). MRI could further be used to determine which samples, and in which regions, of a large part should be tested by 'classical' methods, thus reducing the probability of sampling regions that contain no useful new information about product/process reproducibility or failure mechanisms. Finally, MRI may produce, for each sample imaged, a number of relevant parameters including: distribution of mass fractions of various phases (crystalline, interfacial, amorphous), relaxation time maps of the corresponding phases (related to mechanical properties), void/crack distributions as a function of location in 2-D/3-D and stress distributions. Such NMR studies could assist in the finite element modelling of stress distribution in polymer materials.

4. CONCLUSIONS

The following conclusions can be made based on this work:

- Imaging of rigid semi-crystalline polymers and their corresponding fabricated products is now feasible using large bore magnets.
- Variable temperature MRI under these conditions is both possible and desirable.
- MRI on large samples obviates to some degree the problems associated with sample heterogeneity; a very large sample volume (relative to other methods) can be characterized; visualization of structural differences over large areas or volumes may significantly enhance the studies of failure analysis and process optimization.
- Dynamic tests of stress response of polyolefin products are possible to monitor.

ACKNOWLEDGMENTS

This work was made possible through the assistance and financial support of Nova Chemicals. All MRI measurements were performed in the Petroleum Recovery Institute of Calgary, Alberta, Canada.

REFERENCES

- [1] Axelson, D., Nauerth, A. and Kantzas, A., "Short T₂ Magnetic Resonance Imaging", presented at the 1993 AIChE Spring National Meeting, Houston, TX, March 28 - April 1, 1993.
- [2] Axelson, D.E., Kantzas, A. and Eads, T., "Introduction to Applications of ¹H Magnetic Resonance Imaging of Rigid Solids", *Can J Appl Spec.*, **40**(1), 16-26, 1995.
- [3] Axelson, D.E., Kantzas, A., and Nauerth, A., "¹H Magnetic Resonance Imaging of Rigid Polymeric Solids", *Solid State Nuclear Magnetic Resonance*, **6**(4), 309-321, 1996.
- [4] A. Lustiger, R.L. Markham, "Importance of Tie Molecules in Preventing Polyethylene Fracture Under Long-Term Loading Conditions", *Polymer*, **24**, 1647-1654, 1983.
- [5] W. Browstow, R.D. Corneliussen, "Failure of Plastics", Hanser, Munich, 1986.
- [6] J.G. Williams, "Fracture Mechanics of Polymers", Ellis Horwood Ltd., Chichester, 1984.
- [7] S.K. Battacharya, N. Brown, *J. Mater. Sci.*, **20**, 2767, 1985.
- [8] R.P. Kambour, "Review of Crazing and Fracture in Thermoplastics" *J. Polym. Sci., Macromol. Rev.*, **7**, 1-154, 1973.
- [9] L.C.E. Struik, in "Internal Stresses, Dimensional Instabilities and Molecular Orientations in Plastics", Wiley and Sons, Chichester, 1990.
- [10] P. Blumler, B. Blumich, *Acta Polym.*, **44**, 125, 1993.
- [11] B. Blümich, P. Blümmler, E. Gunther, H.W. Spiess, "Methods and Applications of NMR Imaging in Polymer Research", *Polym. Prepr.*, **31**(1), 579, 1991.
- [12] J.P. Chen-Addad, P. Huchot, A. Viallat, "Proton Magnetic Relaxation Observation of Weak Gel Stretching: Evidence for Affine Deformation", *Polym. Bulletin*, **19**(3), 257-264, 1988.
- [13] A. Marquez-Lucero, C. G'Sell, K.W. Neale, "Experimental Investigation of Neck Propagation in Polymers", *Polymer*, **30**(4), 636-642, 1989.
- [14] V. Nassehi, M. Kinsella, L. Mascia, "Finite Element Modelling of the Stress Distribution in Polymer Composites with Coated Fibre Interlayers", *J. Composite Materials*, **27**(2), 195-214, 1993.
- [15] L.E. Govaert, C.W.M. Bastiaansen, P.J.R. Leblans, "Stress-Strain Analysis of Oriented Polyethylene" *Polymer*, **34**(3), 534-540, 1993.
- [16] P. Jezzard, T.A. Carpenter, L.D. Hall, N.J. Clayden, P. Jackson, "Temperature Mapping in Solid Polymers Using the Temperature Dependence of NMR Relaxation Times", *J. Polym. Sci. B Polym. Phys.*, **30**(12), 1423-1425, 1992.
- [17] J.S. Kauffman and C. Dybowski, "Determination of Transition Temperatures and Crystalline Content of Linear, High Molecular-Weight Polyethylene by Proton NMR Spectroscopy", *J. Polym. Sci., Polym. Phys. Ed.*, **27**(11), 2203-2209, 1989.